Additive Manufacturing 35 (2020) 101405

Contents lists available at ScienceDirect

Additive Manufacturing

journal homepage: www.elsevier.com/locate/addma

Research Paper

Hybrid (3D and inkjet) printed electromagnetic pressure sensor using metamaterial absorber

Heijun Jeong[a,1], Yepu Cui[b,1], Manos M. Tentzeris[b], Sungjoon Lim[a,*]

[a] School of Electrical and Electronics Engineering, Chung-Ang University, Seoul, 06974, Republic of Korea
[b] School of Electrical and Computer Engineering, Georgia Institute of Technology, Atlanta, GA 30332, USA

ARTICLE INFO

Keywords:
Pressure sensor
Metamaterial absorber
Electromagnetic based sensor
3D printing
Inkjet printing

ABSTRACT

This paper proposed a hybrid printed electromagnetic pressure sensor using a metamaterial absorber. We used a three-dimensional printed flexible resin for the transformable substrate with inkjet printed conductive patterns stacked on the printed substrate to realize a hybrid printed electromagnetic pressure sensor. A square ring pattern was implemented for the metamaterial absorber unit cell. Since absorption frequency varied with substrate thickness, the device could be used as an electromagnetic pressure sensor with mechanically transformable substrate. Performance was numerically and experimentally measured, and absorption frequency increased from 5.2 to 5.66 GHz by applying 0 and 20 N pressure, respectively; device sensitivity = 7.75×10^8 Hz/mm (0.2×10^8 Hz/N); and repeatability was retained up to 100 cycles.

1. Introduction

In contrast to components in electronic devices from the 1900s [1–3], modern electronic devices require structures to also be functional components, hence structural electronics have been widely studied recently [4–6]. Structural electronics incorporates printed functional electronic circuits onto irregularly shaped substrates and three-dimensional (3D) structures to realize devices with integrated structures and circuits. Advances in structural electronics technology, such as 3D surface printing [7,8], surface electronics [9,10], in-mould electronics (IME) [11], load bearing supercapacitors [12,13], and energy harvesting skin [14,15] have facilitated rapid customization, material and component cost reduction, and reduced weight and size. Three-dimensional moulded interconnecting devices (3D-MID) [16,17] have also been actively researched because they can overcome various two-dimensional (2D) structural electronics limitations. In particular 2D electronics cannot be applied for 3D structural devices, whereas 3D printed electronics [18,19] can be realized using 3D-MID.

Three-dimensional printing is an excellent candidate to realize 3D-MID. Whull [20] first introduced 3D printing and it offers reduced components and manufacturing processes, such as assembly, work time, and costs; weight and volume; and allows products to be manufactured that cannot be successfully produced using previous approaches. Various 3D printing technologies have been developed, including binder jetting [21,22], material extrusion [23,24], material jetting [25,26], powder bed fusion [27], and vat photopolymerization [28]. Material extrusion and vat photopolymerization methods are typically used for electromagnetic (EM) devices.

Material extrusion, e.g. fused deposition modelling (FDM), melts the construction material and sprays it into position from nozzles to stack them. FDM is the simplest, and hence cheapest, 3D printing method, and can deploy many material filament types, such as poly lactic acid (PLA), acrylonitrile butadiene styrene (ABS), flexible, or metals, using multiple nozzles. However, surface quality is somewhat poor and printing speed is relatively slow.

Vat photopolymerization, e.g. digital light processing (DLP) or stereo lithography (SLA), achieves 3D printing by hardening the resin using projected light. This offers superior print quality and faster printing speed than FDM, and overcomes material extrusion drawbacks. However, vat photopolymerization equipment and materials are relatively expensive.

Conductive materials must be patterned onto 3D structures to realize 3D-MID for electromagnetic applications. Inkjet printing [29] or aerosol jet printing [30,31] are ideal candidate technologies to realize these conductive patterns, and have been employed for various electromagnetic applications [32–34] because it can be applied to a variety of substrates and offers excellent print resolution and accuracy. This additive manufacturing technology also provides a cost-effective,

* Corresponding author.
E-mail address: sungjoon@cau.ac.kr (S. Lim).
[1] Both authors contributed equally to this work.

https://doi.org/10.1016/j.addma.2020.101405
Received 5 April 2020; Received in revised form 6 June 2020; Accepted 19 June 2020
Available online 24 June 2020

simplified fabrication, and eco-friendly process [35] that overcomes many traditional method limitations, such as screen printing [36] or conductive sheet tape [37], which cannot be applied to 3D structural applications.

This paper proposes a hybrid electromagnetic pressure sensor using a metamaterial absorber (MMA). Metamaterials (MMs) can control structural permittivity and permeability by specifically arranging the infinite material periodic structure to be suitable for various electromagnetic applications, such as MM sensors [38], frequency selective structures (FSSs) [39], imaging sensors [40], super lenses [41], high gain antennas [42], terahertz devices [43], etc. They also offer some unique advantages, e.g. MM based wireless electromagnetic sensors can be realized without requiring a transmission line [44–46]. Therefore, we used 3D and inkjet printing conductive patterns to produce a hybrid printed electromagnetic (EM) pressure sensor. We used a 3D printed flexible resin and 3D hinge structure to implement a sensor that can respond to applied pressure. Silver ink based conductive square loops were printed using a Dimatix inkjet printer to supply MMA unit cells on the substrate. We simulated the proposed device using an EM simulator to analyse its structural mechanics and demonstrate the proposed concept. Subsequent experimental verification confirmed that the prototype EM pressure sensor absorption frequency increased from 5.2 to 5.66 GHz when 20 N compressive force was applied, achieving 7.75 × 10^8 Hz/mm (0.2 × 10^8 Hz/N) sensitivity and good repeatability over 100 cycles.

2. Proposed pressure sensor design

Fig. 1 shows the proposed pressure sensor geometry, designed and EM simulated using the ANSYS high frequency structure simulator (HFSS), and intended for fabrication using hybrid additive manufacturing, i.e., inkjet and 3D printing. Conductive patterns were intended to be fabricated from a thin SU-8 dielectric silver ink, considering printing stability. The 3D printed flexible resin for the sensor substrate had dielectric constant = 2.78 and loss tangent = 0.06 [47]. We used aligned holes and screws to control waveguide lateral movement under measurement conditions. Fig. 1(b) and (c) show the defined parameters for the proposed pressure sensor, with dimensions w_s = 88.9 mm, a = 7 mm, b = 39 mm, w = 0.25 mm, ls = 63.5 mm, t_1 = 1 mm, t_2 = 4.5 mm, t_3 = 1 mm, and t_4 = 1 mm.

Fig. 2 shows simulated field distributions and vector current densities for the proposed EM pressure sensor. The waveguide concentrates the electromagnetic wave to the centre, as shown for the unit cell structure in Fig. 2(a). The electric field distribution confirms the proposed EM pressure sensor can control effective permittivity, ε_r. Fig. 2(b) shows that top and bottom surface vector current densities flow in opposite directions, and these antiparallel currents contribute magnetic response, such as effective permeability μ_r.

Absorptivity for the proposed MMA based EM pressure sensor can be expressed as

$$A(\omega) = 1 - \Gamma(\omega) - T(\omega) = 1 - |S_{11}(\omega)|^2 - |S_{21}(\omega)|^2 \quad (1)$$

where T(ω) is the transmission coefficient; and Γ(ω) is the reflection coefficient,

$$\Gamma(\omega) = \frac{Z_0 - Z_M}{Z_0 + Z_M} \quad (2)$$

where Z_0 and Z_M are free space and MM impedance, respectively; and

$$Z_M = \sqrt{\frac{\mu_0 \mu_r}{\varepsilon_0 \varepsilon_r}} \quad (3)$$

where ε_0 and μ_0 are free space, and ε_r and μ_r are MMA permittivity and permeability, respectively. Since the proposed EM pressure sensor is completely covered with conductive ground, T(ω) can be assumed to be zero, and hence the pressure sensor can achieve the highest absorptivity.

From (2), Γ(ω) is minimum when $Z_M = Z_0$ (377 Ω). Fig. 3(a) shows that maximum normalized impedance (Z_M/Z_0) for the proposed EM pressure sensor = 0.8 (real) and -0.15 (imaginary) at 5.3 GHz. Fig. 3(b) shows the proposed EM sensor Γ(ω) = -20 dB and A(ω) = 0.99 (from (1)) at 5.3 GHz.

To verify frequency tunability with pressure, Fig. 4(a) shows simulated EM tunability under compressive force. The proposed EM pressure sensor height deforms depending on applied pressure because the printed resin remains flexible and the substrate structure is deformable with printed hinges with air gap. Therefore, height variation alters the waveguide dimensions and hence proposed EM pressure sensor resonance frequency.

Fig. 4(b) shows the simulated compressive force with respect to compressive length, using COMSOL Multi-physics. We converted the ANSYS HFSS designed structure into stereolithography (STL) file format and imported that into COMSOL Multi-physics. Various analysis parameters for structural compressive forces were set, including Young's modulus (5.6 MPa), Poisson's ratio (0.45), material density (1.05 kg/m^3), and relative permittivity (2.78) [48]. We established that 45 N compressive force was required to increase the compressive length from 0 to 1.0 mm.

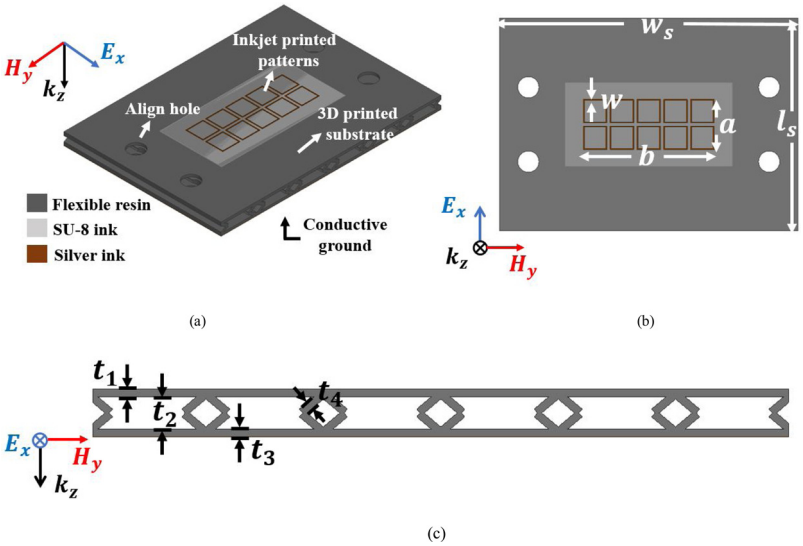

Fig. 1. Proposed electromagnetic pressure sensor geometry (a) perspective, (b) top, and (c) side view.

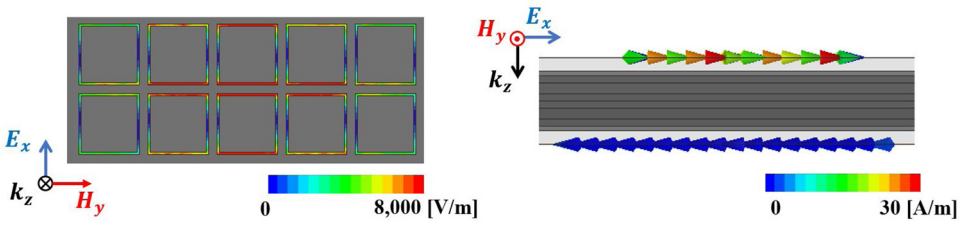

(a) (b)

Fig. 2. Simulated electromagnetic field distributions for the proposed electromagnetic pressure sensor: (a) electric field magnitude and (b) vector current density.

Fig. 4(c) and (d) show reflection coefficients and normalized impedances from ANSYS HFSS confirming that physical changes corresponded to resonance frequency changes. Initial EM pressure sensor resonance = 5.3 GHz, with $\Gamma(\omega)$ = -20 dB and Z_M/Z_0 = 0.8 - j0.15 for h = 6.5 mm. Resonance = 5.5 GHz (0.2 GHz increase) and Z_M/Z_0 = 0.6 - j0.04 for h = 6.3 mm (0.2 mm reduction). Depressing a further 0.2 mm, resonance = 5.6 GHz (0.1 GHz increase) and Z_M/Z_0 = 0.6 + j0.1 for h = 6.1 mm; and resonance = 5.74 GHz, Z_M/Z_0 = 0.6 - j0.4 for h = 5.9 mm.

3. Proposed pressure sensor additive manufacturing process

Fig. 5 shows the proposed hybrid printing fabrication process for the proposed EM sensor comprises

- 3D print dielectric substrate;
- Inkjet print SU-8 dielectric buffer layer to improve surface roughness and conductive layer adhesion; and
- Inkjet print conductive layers and sinter using low temperature gradient.

The substrate was fabricated with a Formlabs Form 2 stereolithography 3D printing system using Formlabs FLGR02 flexible photopolymer resin. This material is a 'rubber-like' elastomer with tensile strength = 7.7–8.5 MPa and 80 % elongation [49]. The material was characterized using the Nicolson-Ross-Weir (NRW) method, with dielectric constant = 2.78 and loss tangent = 0.06 at 5.2 GHz. The substrate comprised a 50 um printed layer and treated following the usual wash and cure post-processing.

- Formlabs Formwash system, 15 min in 91 % isopropyl alcohol to remove remaining resin.
- Formlabs Formcure system, 60 min under 405 nm light at 60°C.

Wash and cure post-processing can dramatically increase printed substrate accuracy, consistency, and structural strength; and reduce electromagnetic losses due to improved polymer cross-linking.

Although the resulting 3D printed substrate exhibited a relatively visually smooth surface, this remained comparatively rough (up to RMS = 42 μm) compared with 0.8 μm thick silver nanoparticle ink conductor layer. Therefore, we first printed a MicroChem SU-8 dielectric buffer layer onto the substrate to reduce surface roughness [50], measuring surface roughness using a KLA Tencor Alpha-step D-100 stylus profilometer. Four SU-8 layers provided a suitably smooth surface (RMS < 1.6 μm). We then cured the printed SU-8 as follows: soft bake at 95°C for 5 min, cure under 254 nm light for 300 mJ/cm^2 energy, then hard bake at 95°C for 10 min.

We adopted 90 s ultraviolent ozone treatment before printing the conductive SNP traces to improve silver nanoparticle ink wettability and adhesion without losing too much resolution. This decreased SNP ink contact angle on the smoothed SU-8 surface from 46° to 29°. Subsequently, we printed 6 SunChemical EMD5730 SNP ink layers using a Dimatix 2800 inkjet printer with 20 μm drop space (1270 dpi).

Generally, EMD5730 SNP inks require high temperature sintering, typically 180°C, for best conductivity and adhesion. However, retaining the 3D printed FLGR02 substrate above 150°C for more than 30 min would dramatically reduce elasticity, causing the substrate to break under compression; and sudden temperature changes can cause substrate shrinkage and hence crack conductor traces. Therefore, we used a low temperature gradient sintering process [51]. The printed substrate was placed on a hot plate, heated from 25°C to 90°C at 150°C/hour, and then held at 90°C for 30 min to completely dry the metallic traces. The

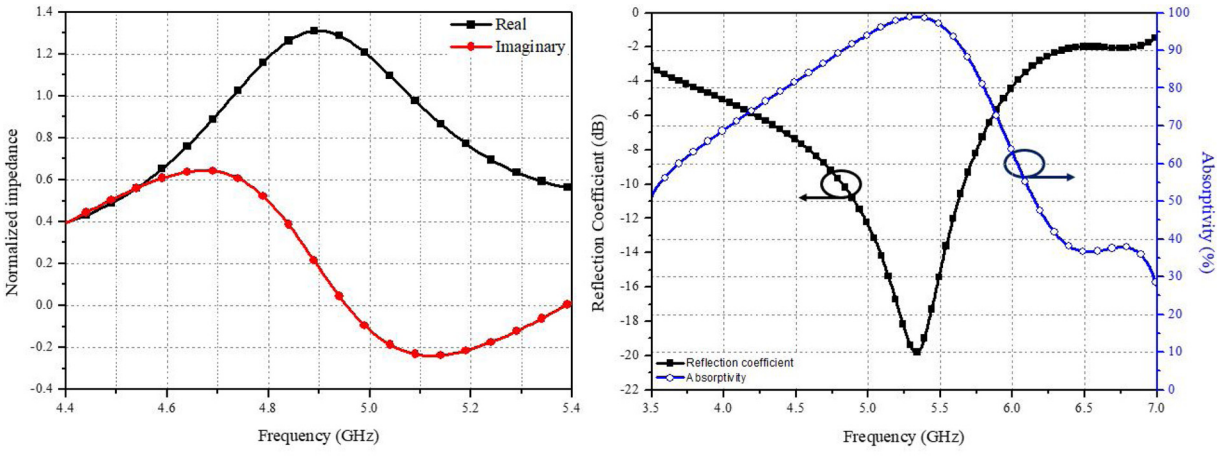

(a) (b)

Fig. 3. Simulation results for the proposed EM pressure sensor: (a) normalized complex impedance and (b) reflection coefficient and absorptivity with respect to frequency.

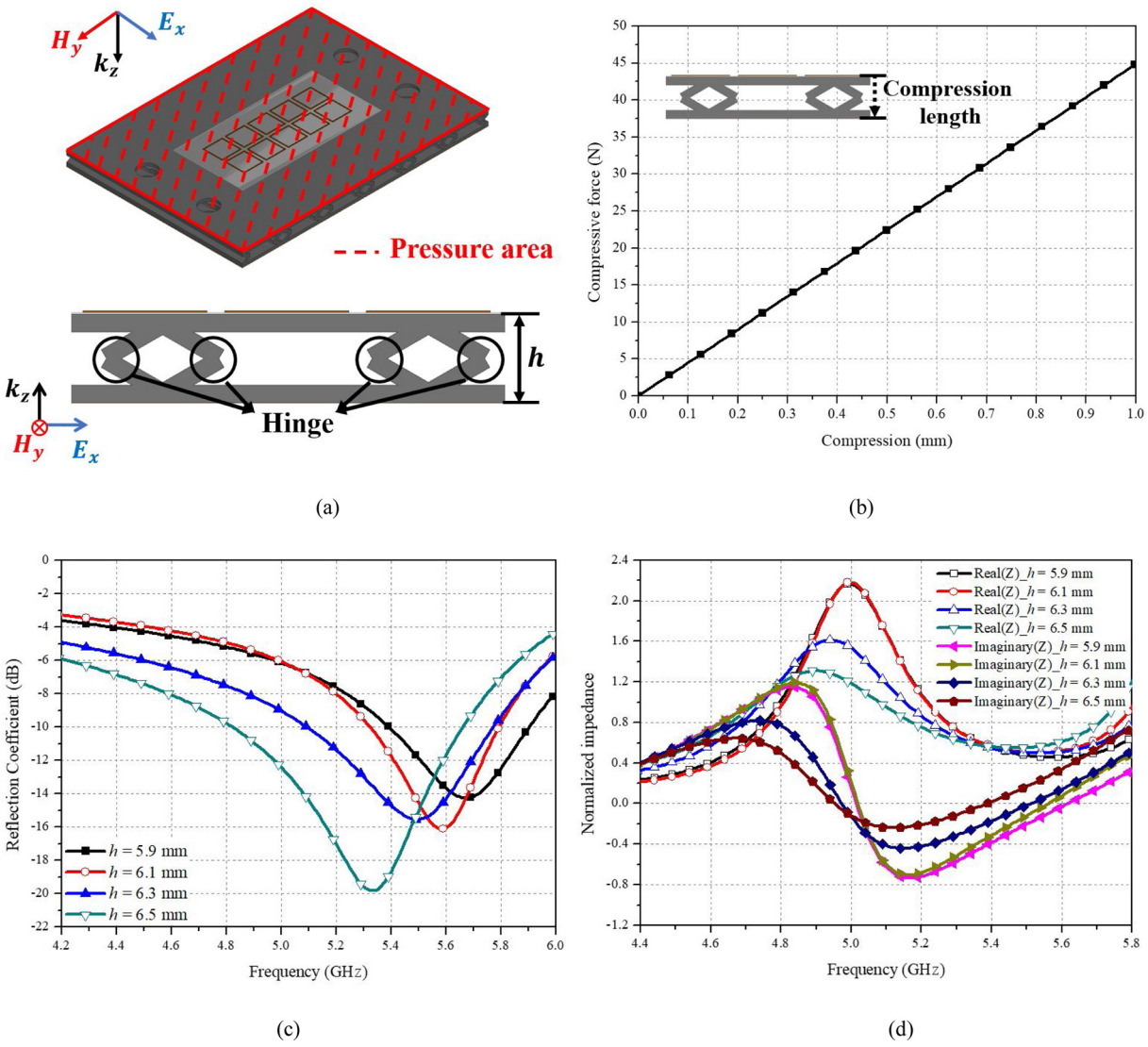

Fig. 4. Simulation results for the proposed EM pressure sensor under compression: (a) pressure area; and (b) compressive force (c) reflection coefficients, and (d) complex impedance with respect to achieved compression (*h* from (a)).

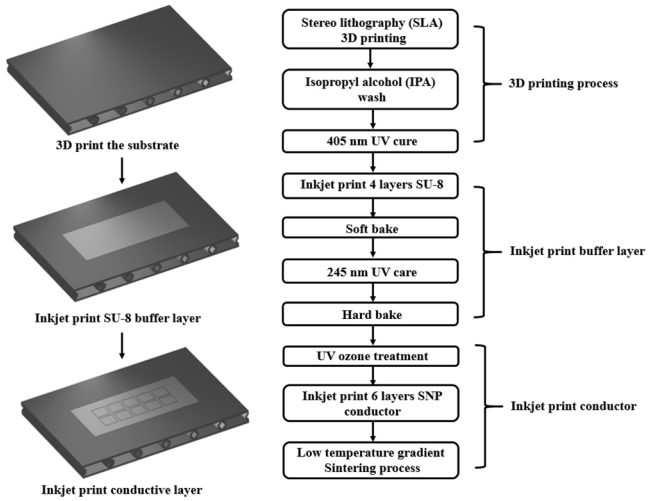

Fig. 5. Fabrication process for the proposed hybrid (3D and inkjet) printed EM sensor.

temperature was then increased to 120°C at 150°C/hour, and held at 120°C for 20 min to sinter the SNP without breaking the 3D printed substrate. Finally, the temperature was reduced to 25°C at 100°C/hour to avoid damage and/or deformation due to sudden temperature change. Fig. 6 confirms the proposed low temperature gradient sintering process produced good uniformity and conductivity (8×10^6 S/m), and Fig. 7 shows the final fabricated EM pressure sensor.

4. Measurement results and discussion

Fig. 8 shows the measured reflection coefficient according to the various heights. The measured initial reflection coefficient of the proposed EM pressure sensor has −16 dB at 5.2 GHz. Next, when the height has been varied by 0.2 mm from 6.5 to 6.3 mm, the absorption frequency has been increased by 0.2 GHz from 5.2 to 5.42 GHz. Then, when the height has been pressured by 0.2 mm from 6.3 to 6.1 mm, the absorption frequency has been increased by 0.13 GHz from 5.42 to 5.55 GHz. Lastly, when the height has been decreased by 0.2 mm from 6.1 to 5.9 mm, the absorption frequency has been increased by 0.11 GHz from 5.55 to 5.66 GHz.

Fig. 9 shows the compressive force measurement setup for the fabricated sample, using and INSTRON 5569 compression

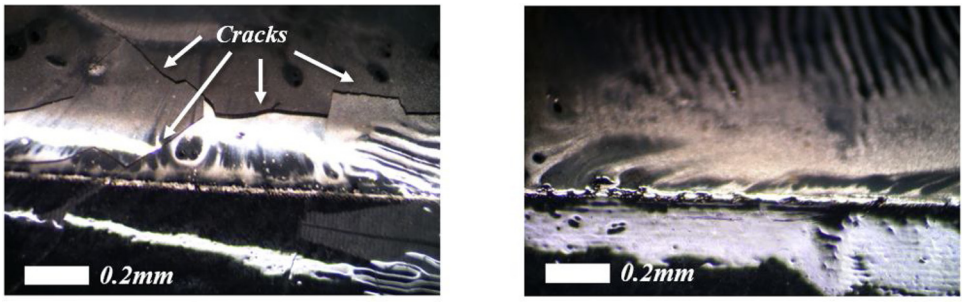

(a) (b)

Fig. 6. Silver ink pathway surface morphology from (a) sintering at 180℃ and (b) low temperature gradient sintering.

(a) (b)

Fig. 7. Fabricated electromagnetic pressure sensor prototype (a) top and (b) side view.

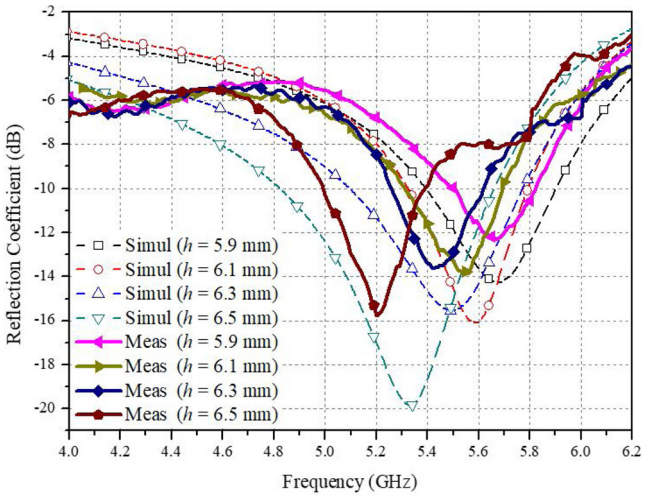

Fig. 8. Results of simulation comparison with reflection coefficients measured at different heights (*h*).

electromechanical device to measure compressive force with respect to compression length. We investigated the mechanical effect of the 3D printed substrate after the thermal sintering which is necessarily for the inkjet printing process. Fig. 9(b) shows the compressive force at different compressive length of the 3D printed substrate with and without the sintering process. Before sintering process, the 3D printed substrate requires compressive force of 17 N to increase compression length from 0 to 0.8 mm. On the other hands, more compressive force of 38 N is required to increase the compression length of the 3D printed substrate from 0 to 0.8 mm. The compressive force is increased after the thermal sintering process because tensile stress and young's modulus of elastomer materials such as rubber are increased [52]."

Fig. 10 shows measured absorption frequency with respect to compressive force and compression length. The proposed EM pressure sensor exhibited resonance at 5.2 GHz for initial zero compressive force; which increased to 5.4 GHz (0.2 GHz) for 2.3 N compressive force applied; and to 5.53 (a further 0.13 GHz) for 8 N compressive force; and finally to 5.66 GHz (a further 0.13 GHz) for 20 N compressive force, as shown in Fig. 11(a) (b) shows the correlation for absorption frequency with compression length. Under initial compression (i.e., zero), the absorption resonance =5.2 GHz, then 5.4, 5.53, and finally 5.66 GHz for 0.2, 0.4, and 0.6 mm compression. Thus, measured absorption resonance can be expressed analytically as $y = 0.775x + 5.25$, where y is resonance, and x is compression length. Hence sensitivity = 7.75×10^8 Hz/mm (0.2×10^8 Hz/N).

Fig. 11 shows the effects of cycling the prototype 300 times, since repeatability is critical for any practical device. Resonance maintained at 5.2 GHz until beyond 100 cycles, with gradual subsequent increased resonance beyond that, reaching 5.3 GHz after approximately 300 cycles as shown in Fig. 11(a). In addition, the conductivity of conducting pattern surface was measured to verify the repeatability of conductivity. Similar with resonance repeatability result, conductivity retains as 6×10^6 S/m until 50 cycles and slightly decreased from 6 to 5×10^6 S/m by 1×10^6 S/m at 100 cycles. From 100 to 300 cycles, the conductivity decreased gradually from 5 to 1.2×10^6 S/m as shown in Fig. 11(b). Thus, the proposed EM pressure sensor maintained consistent performance up to 100 pressure cycles. Table 1 compares the proposed device with several current best practice sensors. The proposed sensor offers simpler fabrication and cost benefits; and the addictive manufacturing fabrication also provides ecological advantages.

5. Conclusions

This paper proposed a hybrid printed electromagnetic pressure sensor using MMA. We employed additive manufacturing, combining 3D and inkjet printing techniques for the substrate and conductive layers, respectively. Flexible resin was used for 3D printing to obtain an approximately linearly compressible structure, with a flexible MMA (silver ink) electromagnetic pattern inkjet printed onto the substrate comprising a series of square loop unit cells over a contiguous conductive ground. Because substrate thickness variation alters the impedance of the MMA, deforming the structure will affect the resonance

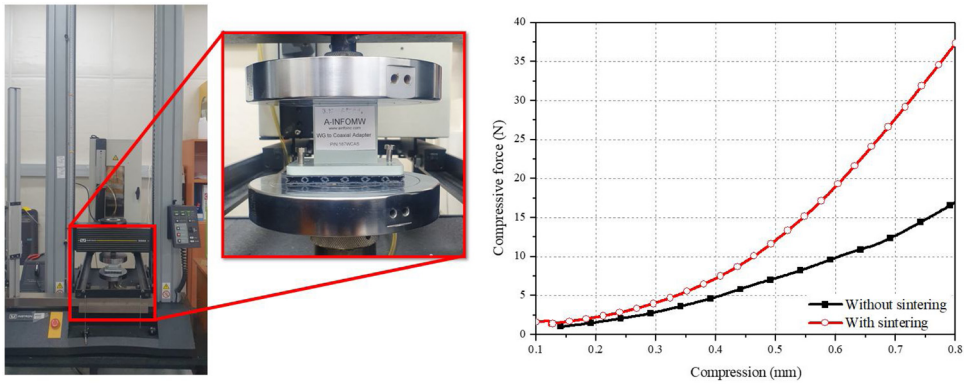

Fig. 9. Compressive force with respect to compression length for the fabricated prototype sensor: (a) measurement setup and (b) measurement results with and without the sintering process.

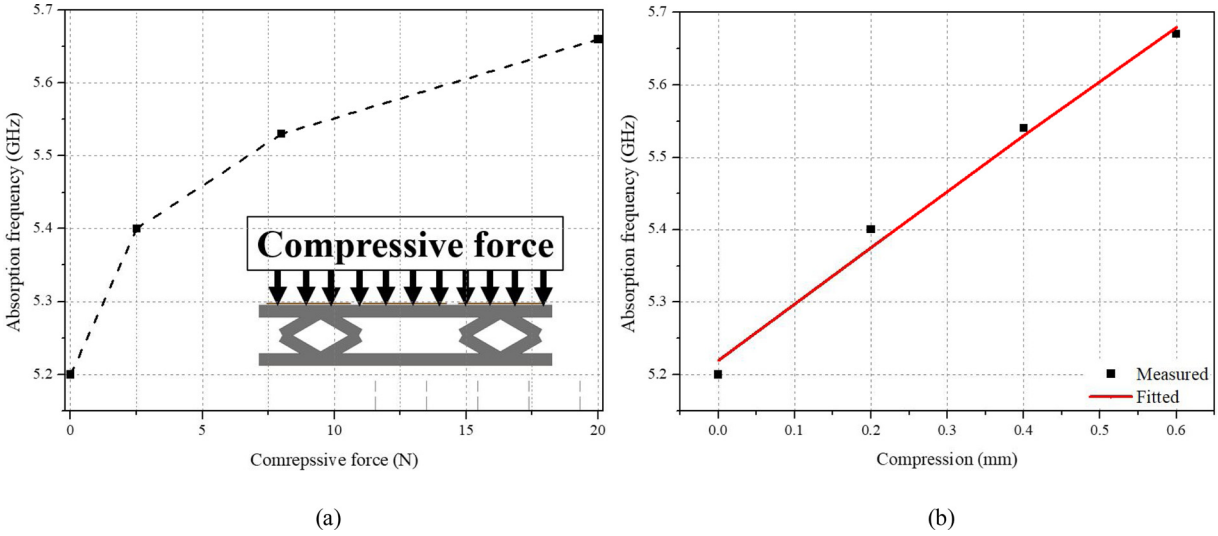

Fig. 10. Measured absorption resonance with respect to (a) compressive force and (b) compression length for the fabricated prototype sensor.

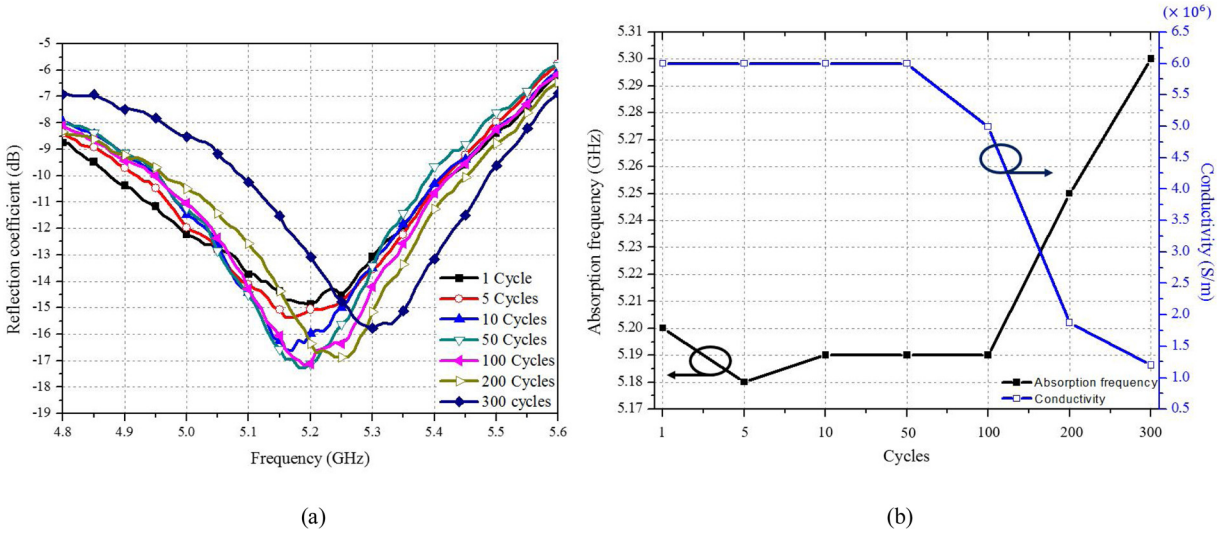

Fig. 11. Fabricated EM pressure sensor repeatability over 300 cycles: (a) measured reflection coefficients and (b) corresponding resonance frequency and resistivity.

Table 1
Proposed and current RF pressure sensor parameters.

Ref	Sensor materials	Operating pressure[a]	Sensitivity[b]	Fabrication method	Cost
[44]	SU-8, Au	0 – 60 mmHg	1.083 MHz/mmHg in air, 683 kHz/mmHg in saline, 120 kHz/mmHg in air	Multiple layer spin coating, photoresist	High
[45]	Polyimide, Au	0 – 213.3 kPa	11.25 kHz/kPa	CEFP (Chip Embedded Flexible Platform)	Moderated
[46]	Si, SiO2, Au, Pyrex, Polyimide, Steel	0 – 50 mmHg	15 kHz/mmHg	MEMS	High
[53]	Biodegradable Polymer, Zn/Fe bilayer conductor	0 – 20 kPa	39 kHz/kPa	MEMS, embossing, multilayer folding, lamination	High
Proposed	Resin, Ag ink	0 – 20 N or 0 – 3.54 kPa	0.2×10^8 Hz/N or 1.13×10^5 kHz/kPa	3D printing, Inkjet printing	Low

[a] 1 mmHg ≈ 133.3 Pa.
[b] 1 MPa = 1 N/mm^2.

frequency in a deterministic manner with respect to overall sensor thickness. Numerical simulations for the proposed sensor were experimentally verified for a fabricated prototype. Applying 20 N pressure changed resonance from 5.2 to 5.66 GHz, with excellent agreement between simulation and experimental results. The proposed EM pressure sensor achieved 7.75 × 10^8 Hz/mm (0.2 × 10^8 Hz/N) sensitivity and consistent outcomes beyond 100 cycles because of the resilience due to the elastic force of the 3D printed substrate material. As a result, the proposed EM pressure sensor has sufficient sensory value and was successfully experimentally validated against numerical simulation. The proposed sensor can be used for a wireless passive pressure sensor by reading the reflected signal. In addition, the proposed hybrid additive manufacturing technique has advantages of the low cost, lightweight and flexibility. As a potential application, the MMA can be deployed to sense the pressure in a large area because it can be ideally extended in infinite size. In addition, we expect that the proposed hybrid fabrication technique can be useful for the integration of the 3D microwave circuits and systems compared with the traditional fabrication technologies such as milling machines [54–56] or manual assembly [57–59].

CRediT authorship contribution statement

Heijun Jeong: Methodology, Validation, Formal analysis, Data curation, Software, Writing - original draft, Writing - review & editing, Visualization. **Yepu Cui:** Methodology, Data curation, Software, Resources, Writing - original draft, Writing - review & editing, Visualization. **Manos M. Tentzeris:** Investigation, Methodology, Resources, Supervision, Project administration. **Sungjoon Lim:** Conceptualization, Methodology, Investigation, Supervision, Project administration, Funding acquisition.

Declaration of Competing Interest

The authors have no conflicting interests.

Acknowledgment

This work was supported by the National Research Foundation of Korea (NRF) grant funded by the Korea government (MSIP) (2017R1A2B3003856) and (MSIT) (2018R1A4A1023826).

Appendix A. Supplementary data

Supplementary material related to this article can be found, in the online version, at doi:https://doi.org/10.1016/j.addma.2020.101405.

References

[1] D. Chiozzi, M. Bernardoni, N. Delmonte, P. Cova, A simple 1-D finite elements approach to model the effect of PCB in electronic assemblies, Microelectron. Reliab. 58 (2016) 126–132, https://doi.org/10.1016/j.microrel.2015.11.029.
[2] A. Baïri, Quantification of the natural convective heat transfer for the tilted and wire-bonded QFN32b-PCB electronic assembly, Int. Commun. Heat Mass Transf. 72 (2016) 84–89, https://doi.org/10.1016/j.icheatmasstransfer.2016.01.011.
[3] A. Baïri, O. Haddad, Detailed correlations on natural convective heat transfer coefficients for a QFN32 electronic device on inclined PCB, Numer. Heat Transf. Part A Appl. 69 (2016) 841–849, https://doi.org/10.1080/10407782.2015.1090850.
[4] E. MacDonald, R. Salas, D. Espalin, M. Perez, E. Aguilera, D. Muse, R.B. Wicker, 3D printing for the rapid prototyping of structural electronics, IEEE Access 2 (2014) 234–242, https://doi.org/10.1109/ACCESS.2014.2311810.
[5] G.L. Goh, S. Agarwala, G.D. Goh, H.K.J. Tan, L. Zhao, T.K. Chuah, W.Y. Yeong, Additively manufactured multi-material free-form structure with printed electronics, Int. J. Adv. Manuf. Technol. 94 (2018) 1309–1316, https://doi.org/10.1007/s00170-017-0972-z.
[6] A.J. Lopes, E. MacDonald, R.B. Wicker, Integrating stereolithography and direct print technologies for 3D structural electronics fabrication, Rapid Prototyp. J. 18 (2012) 129–143, https://doi.org/10.1108/13552541211212113.
[7] F. Kotz, K. Arnold, W. Bauer, D. Schild, N. Keller, K. Sachsenheimer, T.M. Nargang, C. Richter, D. Helmer, B.E. Rapp, Three-dimensional printing of transparent fused

silica glass, Nature 544 (2017) 337–339, https://doi.org/10.1038/nature22061.
[8] J.J. Adams, E.B. Duoss, T.F. Malkowski, M.J. Motala, B.Y. Ahn, R.G. Nuzzo, J.T. Bernhard, J.A. Lewis, Conformal printing of electrically small antennas on three-dimensional surfaces, Adv. Mater. 23 (2011) 1335–1340, https://doi.org/10.1002/adma.201003734.
[9] L. Ljungkrona, Z. Lai, Development of conductive adhesive joining for surface-mounting electronics manufacturing, IEEE Trans. Compon. Packag. Manuf. Technol. Part B 18 (1995) 313–319, https://doi.org/10.1109/96.386267.
[10] Q. Cao, S.J. Han, G.S. Tulevski, Y. Zhu, D.D. Lu, W. Haensch, Arrays of single-walled carbon nanotubes with full surface coverage for high-performance electronics, Nat. Nanotechnol. 8 (2013) 180–186, https://doi.org/10.1038/nnano.2012.257.
[11] T.Y. Lin, B. Njoman, D. Crouthamel, K.H. Chua, S.Y. Teo, Y.Y. Ma, The impact of moisture in mold compound preforms on the warpage of PBGA packages, Microelectron. Reliab. 44 (2004) 603–609, https://doi.org/10.1016/j.microrel.2003.08.003.
[12] N. Shirshova, A. Bismarck, S. Carreyette, Q.P.V. Fontana, E.S. Greenhalgh, P. Jacobsson, P. Johansson, M.J. Marczewski, G. Kalinka, A.R.J. Kucernak, J. Scheers, M.S.P. Shaffer, J.H.G. Steinke, M. Wienrich, Structural supercapacitor electrolytes based on bicontinuous ionic liquid-epoxy resin systems, J. Mater. Chem. A. 1 (2013) 15300–15309, https://doi.org/10.1039/c3ta13163g.
[13] A.S. Westover, J.W. Tian, S. Bernath, L. Oakes, R. Edwards, F.N. Shabab, S. Chatterjee, A.V. Anilkumar, C.L. Pint, A multifunctional load-bearing solid-state supercapacitor, Nano Lett. 14 (2014) 3197–3202, https://doi.org/10.1021/nl500531r.
[14] Y. Yang, H. Zhang, Z.H. Lin, Y.S. Zhou, Q. Jing, Y. Su, J. Yang, J. Chen, C. Hu, Z.L. Wang, Human skin based triboelectric nanogenerators for harvesting biomechanical energy and as self-powered active tactile sensor system, ACS Nano 7 (2013) 9213–9222, https://doi.org/10.1021/nn403838y.
[15] S. Lee, B.D. Youn, A new piezoelectric energy harvesting design concept: multimodal energy harvesting skin, IEEE Trans. Ultrason. Ferroelectr. Freq. Control 58 (2011) 629–645, https://doi.org/10.1109/TUFFC.2011.5733266.
[16] B. Bachy, R. Süß-Wolf, L. Wang, Z. Fu, N. Travitzky, P. Greil, J. Franke, Novel ceramic-based material for the applications of molded interconnect devices (3D-MID) based on laser direct structuring, Adv. Eng. Mater. 20 (2018) 1–10, https://doi.org/10.1002/adem.201700824.
[17] N. Bachnak, 3D-MID technology MEMS connectivity at system level, Proc. 2012 IEEE 14th Electron. Packag. Technol. Conf. EPTC 2012, 2012, pp. 572–576, , https://doi.org/10.1109/EPTC.2012.6507147.
[18] M. Areir, Y. Xu, D. Harrison, J. Fyson, R. Zhang, Development of 3D printing technology for the manufacture of flexible electric double-layer capacitors, Mater. Manuf. Process. 33 (2018) 905–911, https://doi.org/10.1080/10426914.2017.1401712.
[19] J.C.S. Chieh, B. Dick, S. Loui, J.D. Rockway, Development of a ku-band corrugated conical horn using 3-d print technology, IEEE Antennas Wirel. Propag. Lett. 13 (2014) 201–204, https://doi.org/10.1109/LAWP.2014.2301169.
[20] C.W. Hull, The birth of 3D printing, Res. Technol. Manag. 58 (2015) 25–29, https://doi.org/10.5437/08956308X5806067.
[21] N. Afshar-Mohajer, C.Y. Wu, T. Ladun, D.A. Rajon, Y. Huang, Characterization of particulate matters and total VOC emissions from a binder jetting 3D printer, Build. Environ. 93 (2015) 293–301, https://doi.org/10.1016/j.buildenv.2015.07.013.
[22] S.M. Gaytan, M.A. Cadena, H. Karim, D. Delfin, Y. Lin, D. Espalin, E. MacDonald, R.B. Wicker, Fabrication of barium titanate by binder jetting additive manufacturing technology, Ceram. Int. 41 (2015) 6610–6619, https://doi.org/10.1016/j.ceramint.2015.01.108.
[23] A.R. Torrado, C.M. Shemelya, J.D. English, Y. Lin, R.B. Wicker, D.A. Roberson, Characterizing the effect of additives to ABS on the mechanical property anisotropy of specimens fabricated by material extrusion 3D printing, Addit. Manuf. 6 (2015) 16–29, https://doi.org/10.1016/j.addma.2015.02.001.
[24] S.I. Park, D.W. Rosen, S. kyum Choi, C.E. Duty, Effective mechanical properties of lattice material fabricated by material extrusion additive manufacturing, Addit. Manuf. 1 (2014) 12–23, https://doi.org/10.1016/j.addma.2014.07.002.
[25] J. Dilag, T. Chen, S. Li, S.A. Bateman, Design and direct additive manufacturing of three-dimensional surface micro-structures using material jetting technologies, Addit. Manuf. 27 (2019) 167–174, https://doi.org/10.1016/j.addma.2019.01.009.
[26] Y.L. Yap, C. Wang, S.L. Sing, V. Dikshit, W.Y. Yeong, J. Wei, Material jetting additive manufacturing: an experimental study using designed metrological benchmarks, Precis. Eng. 50 (2017) 275–285, https://doi.org/10.1016/j.precisioneng.2017.05.015.
[27] W.E. King, H.D. Barth, V.M. Castillo, G.F. Gallegos, J.W. Gibbs, D.E. Hahn, C. Kamath, A.M. Rubenchik, Observation of keyhole-mode laser melting in laser powder-bed fusion additive manufacturing, J. Mater. Process. Technol. 214 (2014) 2915–2925, https://doi.org/10.1016/j.jmatprotec.2014.06.005.
[28] J.S. Yun, T.W. Park, Y.H. Jeong, J.H. Cho, Development of ceramic-reinforced photopolymers for SLA 3D printing technology, Appl. Phys. A Mater. Sci. Process. 122 (2016) 1–6, https://doi.org/10.1007/s00339-016-0157-x.
[29] G.L. Goh, J. Ma, K.L.F. Chua, A. Shweta, W.Y. Yeong, Y.P. Zhang, Inkjet-printed patch antenna emitter for wireless communication application, Virtual Phys. Prototyp. 11 (2016) 289–294, https://doi.org/10.1080/17452759.2016.1229802.
[30] F. Cai, S. Pavlidis, J. Papapolymerou, Y.H. Chang, K. Wang, C. Zhang, B. Wang, Aerosol jet printing for 3-D multilayer passive microwave circuitry, Eur. Microw. Week 2014 Connect. Futur. EuMW 2014 - Conf. Proceedings; EuMC 2014 44th Eur. Microw. Conf. European Microwave Association, 2014, pp. 512–515, , https://doi.org/10.1109/EuMC.2014.6986483.
[31] D. Jahn, R. Eckstein, L.M. Schneider, N. Born, G. Hernandez-Sosa, J.C. Balzer, I. Al-Naib, U. Lemmer, M. Koch, Digital aerosol jet printing for the fabrication of terahertz metamaterials, Adv. Mater. Technol. 3 (2018) 1–6, https://doi.org/10.1002/admt.201700236.
[32] D. Lee, H.K. Sung, S. Lim, Flexible subterahertz metamaterial absorber fabrication using inkjet printing technology, Appl. Phys. B Lasers Opt. 122 (2016) 1–8, https://doi.org/10.1007/s00340-016-6482-0.
[33] S. Choi, S. Eom, M.M. Tentzeris, S. Lim, Inkjet-printed electromagnet-based touchpad using spiral resonators, J. Microelectromech. Syst. 25 (2016) 947–953, https://doi.org/10.1109/JMEMS.2016.2593956.
[34] Y. Xu, X. Wu, X. Guo, B. Kong, M. Zhang, X. Qian, S. Mi, W. Sun, The boom in 3D-printed sensor technology, Sensors (Basel) 17 (2017) 1–37, https://doi.org/10.3390/s17051166.
[35] A. Salim, S. Lim, Review of recent inkjet-printed capacitive tactile sensors, Sensors (Switzerland) 17 (2017) 2593, https://doi.org/10.3390/s17112593.
[36] H. Jeong, S. Lim, A stretchable electromagnetic absorber fabricated using screen printing technology, Sensors 17 (2017) 1175–1184, https://doi.org/10.3390/s17051175.
[37] S.I.H. Shah, S. Lim, Bioinspired DNA origami quasi-Yagi helical antenna with beam direction and beamwidth switching capability, Sci. Rep. 9 (2019) 1–9, https://doi.org/10.1038/s41598-019-50893-8.
[38] R. Melik, E. Unal, N. Kosku Perkgoz, C. Puttlitz, H.V. Demir, Flexible metamaterials for wireless strain sensing, Appl. Phys. Lett. 95 (2009) 2–5, https://doi.org/10.1063/1.3250175.
[39] T.R. Cameron, G.V. Eleftheriades, Analysis and characterization of a wide-angle impedance matching metasurface for dipole phased arrays, IEEE Trans. Antennas Propag. 63 (2015) 3928–3938, https://doi.org/10.1109/TAP.2015.2448231.
[40] T. Chen, S. Li, H. Sun, Metamaterials application in sensing, Sensors. 12 (2012) 2742–2765, https://doi.org/10.3390/s120302742.
[41] A.K. Iyer, G.V. Eleftheriades, Mechanisms of subdiffraction free-space imaging using a transmission-line metamaterial superlens: an experimental verification, Appl. Phys. Lett. 92 (2008) 1–4, https://doi.org/10.1063/1.2904635.
[42] M. Sun, Z.N. Chen, X. Qing, Gain enhancement of 60-GHz antipodal tapered slot antenna using zero-index metamaterial, IEEE Trans. Antennas Propag. 61 (2013) 1741–1746, https://doi.org/10.1109/TAP.2012.2237154.
[43] H.T. Chen, W.J. Padilla, J.M.O. Zide, A.C. Gossard, A.J. Taylor, R.D. Averitt, Active terahertz metamaterial devices, Nature 444 (2006) 597–600, https://doi.org/10.1038/nature05343.
[44] N. Xue, S.P. Chang, J.B. Lee, A SU-8-based microfabricated implantable inductively coupled passive RF wireless intraocular pressure sensor, J. Microelectromech. Syst. 21 (2012) 1338–1346, https://doi.org/10.1109/JMEMS.2012.2206072.
[45] K.H. Shin, C.R. Moon, T.H. Lee, C.H. Lim, Y.J. Kim, Flexible wireless pressure sensor module, Sens. Actuators A Phys. 123–124 (2005) 30–35, https://doi.org/10.1016/j.sna.2005.01.008.
[46] G. Chitnis, T. Maleki, B. Samuels, L.B. Cantor, B. Ziaie, A minimally invasive implantable wireless pressure sensor for continuous IOP monitoring, IEEE Trans. Biomed. Eng. 60 (2013) 250–256, https://doi.org/10.1109/TBME.2012.2205248.
[47] W. Su, Z. Wu, Y. Fang, R. Bahr, P.M. Raj, R. Tummala, M.M. Tentzeris, 3D printed wearable flexible SIW and microfluidics sensors for Internet of Things and smart health applications, IEEE MTT-S Int. Microw. Symp. Dig. (2017) 544–547, https://doi.org/10.1109/MWSYM.2017.8058621.
[48] J.R.C. Dizon, A.H. Espera, Q. Chen, R.C. Advincula, Mechanical characterization of 3D-printed polymers, Addit. Manuf. 20 (2018) 44–67, https://doi.org/10.1016/j.addma.2017.12.002.
[49] Using flexible resin, (n.d.).? https://support.formlabs.com/s/article/Using-Flexible-Resin?language=en_US (Accessed 5 March 2020).
[50] B.K. Tehrani, B.S. Cook, M.M. Tentzeris, Inkjet-printed 3D interconnects for millimeter-wave system-on-package solutions, IEEE MTT-S Int. Microw. Symp. Dig., IEEE (2016) 1–4, https://doi.org/10.1109/MWSYM.2016.7540084.
[51] Y. Cui, S.A. Nauroze, M.M. Tentzeris, Novel 3D-Printed reconfigurable origami frequency selective surfaces with flexible inkjet-printed conductor traces, IEEE MTT-S Int. Microw. Symp. Dig. (2019) 1367–1370, https://doi.org/10.1109/mwsym.2019.8700994.
[52] M.A. Campeau, A. Lortie, P. Tremblay, M.O. Béliveau, D. Dubé, È. Langelier, L. Rouleau, Effect of manufacturing and experimental conditions on the mechanical and surface properties of silicone elastomer scaffolds used in endothelial mechanobiological studies, Biomed. Eng. Online 16 (2017) 1–23, https://doi.org/10.1186/s12938-017-0380-5.
[53] M. Luo, A.W. Martinez, C. Song, F. Herrault, M.G. Allen, A microfabricated wireless RF pressure sensor made completely of biodegradable materials, J. Microelectromech. Syst. 23 (2014) 4–13, https://doi.org/10.1109/JMEMS.2013.2290111.
[54] X. Shang, M. Lancaster, Y.L. Dong, W-band waveguide filter based on large TM120 resonators to ease CNC milling, Electron. Lett. 53 (2017) 488–490, https://doi.org/10.1049/el.2016.4131.
[55] X.T.A. Chu, B.N. Ta, L.T.H. Ngo, M.H. Do, P.X. Nguyen, D.N.H. Nam, Microwave absorption properties of iron nanoparticles prepared by ball-milling, J. Electron. Mater. 45 (2016) 2311–2315, https://doi.org/10.1007/s11664-015-4248-9.
[56] R. Antonije, O. Djordjevic, I. Dragan, A.G. Zajic, Modeling and design of milled microwave printed circuit boards, Microw. Opt. Technol. Lett. 53 (2011) 264–270, https://doi.org/10.1002/mop.25724.
[57] M. Nowottnick, R. Diehm, Soldering technology for 3D PCB assemblies with microwave heating, IEEE Int. Symp. Ind. Electron. (2007) 3273–3277, https://doi.org/10.1109/ISIE.2007.4375139.
[58] M.I.M. Ghazali, E. Gutierrez, J.C. Myers, A. Kaur, B. Wright, P. Chahal, Affordable 3D printed microwave antennas, Proc. - Electron. Components Technol. Conf. IEEE, 2015, pp. 240–246, , https://doi.org/10.1109/ECTC.2015.7159599.
[59] G.W. Dahlmann, E.M. Yeatman, P. Young, I.D. Robertson, S. Lucyszyn, Fabrication, RF characteristics and mechanical stability of self-assembled 3D microwave inductors, Sens. Actuators A Phys. 97–98 (2002) 215–220, https://doi.org/10.1016/S0924-4247(01)00851-2.